Available online at www.sciencedirect.com

SciVerse ScienceDirect

Journal of the European Ceramic Society 32 (2012) 2957–2964

www.elsevier.com/locate/jeurceramsoc

Transparent YAG obtained by spark plasma sintering of co-precipitated powder. Influence of dispersion route and sintering parameters on optical and microstructural characteristics

Giulia Spina [a,*], Guillaume Bonnefont [b], Paola Palmero [a], Gilbert Fantozzi [b], Jérome Chevalier [b], Laura Montanaro [a]

[a] *Department of Material Science and Chemical Engineering, Politecnico di Torino, INSTM, R.U. PoliTO, LINCE Lab., C.so Duca degli Abruzzi 24, 10129 Torino, Italy*

[b] *Université de Lyon, INSA de Lyon, MATEIS UMR CNRS 5510, Bât. Blaise Pascal, 7, Av. Jean Capelle, 69621 Villeurbanne, France*

Received 31 August 2011; received in revised form 22 February 2012; accepted 27 February 2012
Available online 23 March 2012

Abstract

A fine-grained (330 nm) yttrium aluminium garnet (YAG) ceramic, presenting a non-negligible transparency (66% RIT at 600 nm), was obtained by spark plasma sintering. The YAG powder was manufactured by co-precipitation, starting from a yttrium and aluminium chlorides solution. A soft precursor was obtained, whose phase evolution was studied by X-ray diffraction. Calcined powders were dispersed by either ball milling or by ultrasonication and then subjected to spark plasma sintering at several temperatures (1200–1400 °C) and for a reduced time (15 min). It is shown that the dispersion method plays a key role in enhancing the optical characteristics of YAG ceramics, in order to obtain a material with a small grain size, transparent in both the visible and the infrared range.

Keywords: YAG; Transparency; SPS; Dispersion; Annealing

1. Introduction

Fully dense polycrystalline $Y_3Al_5O_{12}$ (YAG) is a suitable transparent material for harsh environments, withstanding high temperatures (melting point 1940 °C) and corrosive conditions. It is an oxide ceramic with outstanding functional and mechanical properties, exhibiting high temperature strength, low creep rate and good mechanical properties.[1,2] When doped with rare earth elements, YAG is optically active and used in a variety of applications.[3,4]

Synthesis of highly pure YAG powder has been accomplished by several wet-chemical methods.[5–7] Agglomeration of the calcined powder is often an issue and it has been tackled by using water scavenging solvents,[8] dispersants[9,10] and freeze drying,[11,12] or reduced by ball milling with alumina spheres, for several hours.[13]

Polycrystalline transparent YAG has been successfully produced by vacuum sintering; the fully dense bodies usually present a mean grain size of about 10 μm,[13–16] which is narrowed to about 3 μm only in a limited number of cases.[5,17] In order to reduce the YAG grain size, thus to improve its mechanical properties, such as the thermal shock resistance, and to limit thermally induced birefringence for laser application,[18] free sintering followed by hot isostatic pressing (HIP) and spark plasma sintering (SPS) were also tested.[19,20] In Table 1 are reported some of the literature results for YAG and Nd:YAG, in terms of real in-line transmission (RIT) and grain size.

SPS, also known as field assisted sintering (FAST), is an emerging consolidation technique which combines pulsed electric currents and uniaxial compaction. In the last few years it has become possible to obtain fine and dense materials using SPS.[21,22] With respect to other advances sintering techniques, such as vacuum sintering or HIP, SPS offers considerable advantages, such as short sintering time and, generally, lower sintering temperatures, leading to finer microstructure.[23] Additionally, the very short SPS sintering time, often in the range of minutes,[12,24]

* Corresponding author.
E-mail address: giulia.spina@polito.it (G. Spina).

0955-2219/$ – see front matter © 2012 Elsevier Ltd. All rights reserved.
doi:10.1016/j.jeurceramsoc.2012.02.052

Table 1
Real in-line transmission (RIT), at 600 nm and 1064 nm, and grain size for transparent YAG sintered by various techniques.

Material	Powder	Manufacturing technique	Additives	RIT @ 600 nm (%)	RIT @ 1064 nm (%)	Grain size (μm)	Thickness (mm)	Reference
Nd:YAG	Co-precipitated	Vacuum sintering, SiO_2 doping	SiO_2 0.035 wt% (TEOS)		∼85	2.8	1	Stevenson et al.[17]
Nd:YAG	Commercial (Sumitomo Chemical Co., Shin-Etsu Co., Nippon Yttrium Co.)	Free sintering + hot isostatic pressing	SiO_2 0.06 wt% (TEOS)		84	2–3	Undecl.	Lee et al.[19]
Nd:YAG	Co-precipitated	Slip casting + vacuum sintering	Undeclared binder and dispersant	Undecl., high	Undecl., high	3, 4, 7.5	Undecl.	Yagi et al.[5]
YAG	Commercial powder (Alumina, Sumitomo Chemical Co.), co-precipitated (Yttria)	Vacuum sintering + annealing	TEOS 0.5 wt%	75		∼7		Gong et al.[14]
Nd:YAG	Co-precipitated, freeze dried	Free sintering + hot isostatic pressing	None	56	∼80	7–8	0.8	Suárez et al.[25]
Nd:YAG	Commercial powders (Baikowsky, Taimei, Cerox), spray dryed	Vacuum sintering + annealing	TEOS 0.5 wt%		∼78	∼10	3	Esposito et al.[13]
Nd:YAG	Co-precipitated	Slip casting + vacuum sintering	Undeclared binder and dispersant		∼84	10	104	Jianren Lu et al.[15]
Nd:YAG	Co-precipitated	Vacuum sintering + annealing	MgO 0.01 wt%, TEOS 0.5 wt%	78.68 (400 nm)	82.58	>15	3	Liu et al.[16]
YAG	Co-precipitated, oven dried	SPS	None	Negligible (680 nm)	40	0.42	0.8	Suarez et al.[12]
YAG	Co-precipitated, freeze dried	SPS	None	56 (680 nm)	82	0.38	0.8	Suarez et al.[12]
YAG	Commercial (Nanocerox, 50 nm average size)	SPS	None	∼20 (500 nm)	∼42 (1000 nm)	∼0.15	4	Frage et al.[20]
YAG	Commercial (Nanocerox)	SPS	LiF	∼73 (500 nm)	∼82 (1000 nm)	∼1.5	4	Frage et al.[20]
YAG	Commercial (Tal materials, 34 nm average size)	SPS	None	1.1		∼0.5	0.5	Chaim et al. [24]

allows to easily test the sinterability of different powders, and is therefore suitable for fast comparative studies.

In the past, few researchers have investigated the spark plasma sintering of transparent YAG ceramics.[12,20,24] In all cases, the powders were directly poured in the SPS graphite die, without any specific preparation, i.e. no shape forming nor particle size refinement procedure was set out.

Thus, the objective of the present paper is to:

(1) demonstrate that a fine grained, transparent YAG ceramics can be obtained by spark plasma sintering, with neither dispersants nor sintering aids,
(2) highlight the critical importance of powder processing on the sintering behaviour, the final microstructure and the related optical properties.

2. Material and methods

YAG powder was synthesized by the co-precipitation route, starting from a mixed aqueous solution of yttrium and aluminium chlorides. This solution was added drop-wise to an aqueous solution of ammonium hydrogen carbonate, under mild agitation at room temperature. Then the slurry was aged for 24 h, until its pH rose from 7.5 to 9. The precipitate was then washed by centrifugation several times, in distilled water and in absolute ethanol (98.9%). It was finally dried for 2 days in an oven at 60 °C, resulting in a soft cake, easily crushed in an agate mortar.

Simultaneous DTA–TG analysis (Netzsch STA409) was performed on a powdered sample of about 150 mg, up to 1400 °C in static air, with a heating rate of 10 °C/min.

The dried powder was submitted to thermal treatments in a box furnace, in the temperature range 900–1200 °C, for 30 min, and its phase evolution was followed by X-ray diffraction (XRD, Bruker D8 Advance).

The phase evolution of the dried precursor was also followed by high temperature X-ray diffraction (HT-XRD), in the range 850–1000 °C, with a temperature step of 25 °C.

On the basis of these analyses, the powders were calcined in a box furnace at 1000 °C for 30 min, in air, with a heating rate of 10 °C/min.

Two dispersion routes were tested, precisely ball milling (BM) and ultrasonication (US). Ball milling was carried out by using alumina spheres (purity > 95 wt%) with a Gaussian diameter distribution around 1.5 mm. Weight ratio powder/spheres was 1:10. Solid load of the slurry was 33 wt%. Approximately 6 h of milling were necessary to fully disperse the particles. The dispersion process by ultrasonication required 1 h, during which the ultrasonic pump was operative 50% of the time, in order to avoid heating of the slurry. Absolute ethanol was used as a dispersion media for all the studies. The evolution of the particle size distribution was followed by laser granulometry (Mastersizer 2000, Malvern).

After dispersion, the powders were subjected to flotation for 24 h in 200 ml ethanol, in order to avoid any residual coarse particles.[26]

Finally, drying was performed by rotative evaporation, at 60 °C and 200 mbar pressure.

After being poured into a graphite die of 20 mm diameter, the processed powders were sintered into an SPS equipment HPD 25/2 (FCT, Germany), under low vacuum (0.1 mbar) at a constant pressure of 74 MPa. The SPS cycles were constructed as follows: a fast heating rate (100 °C/min) up to 1100 °C, then a relatively slow heating rate (8 °C/min) up to the sintering temperature, followed by an isothermal step of 15 min. The sintering temperature was varied between 1200 °C and 1400 °C, while all other parameters were kept constant.

After polishing on both sides up to 1 μm diamond paste, transparency measurements were performed by using a spectrophotometer UV/Vis NIR V-670 (Jasco, Japan) in the wavelength range from 300 nm to 2500 nm. Transmittance results T_s were recorded on samples of different thicknesses t_s and then normalised to the desired thickness t of 1.5 mm by using the formula:

$$T = T_{th}\left(\frac{T_s}{T_{th}}\right)^{t/ts},$$

where T_{th} is the YAG theoretical transmittance at the given wavelength.

SEM and TEM micrographs were performed with a Zeiss Supra 55VP and a Hitachi S2300 microscope. Each polished sample was chemically etched with boiling phosphoric acid for 15 s in order to evidence the grain boundaries. For each grain size calculation more than 150 grains were measured. The correction factor 1.225 was applied, as explained in the work by Apetz and van Bruggen.[27] Thermal etching, 50 °C lower than the sintering temperature, was also performed on some of the samples.

Subsequent annealing were performed in air, for 1 h at increasing temperatures, measuring the transmittance after each treatment, in order to follow its evolution as a function of the temperature.

3. Results

The as-dried precursor was completely amorphous, as stated by XRD analysis. No crystalline phases were detected up to 850 °C, whereas the presence of YAG (JCPDS reference 33-0040) as well as of the hexagonal transition phase $YAlO_3$ (JCPDS reference 74-1334) was found at 875 °C by HT-XRD (Fig. 1). Starting from 950 °C, pure YAG was present.

The DTA–TG curves for the as-synthesized powder are reported in Fig. 2. The TG curve shows that the precursor completely decomposes below 1100 °C, with an overall weight loss of approximately 43.4%. Much of this weight loss took place below 400 °C, corresponding to about 70% of total weight loss.

The formation of YAG phase is usually found in the literature as a sharp exothermic peak in the DTA curve.[5,16] However, here two exothermic peaks at 918 °C and 1032 °C are observed. On the basis of the previously reported XRD results, the former exothermal signal can be reasonably imputed to the almost simultaneous crystallization of YAG and $YAlO_3$ phases, the latter to the transformation of the metastable $YAlO_3$ into the final, stable YAG phase. This behaviour is similar to the one observed by Li et al.[28] when ammonia water was used as a precipitant.

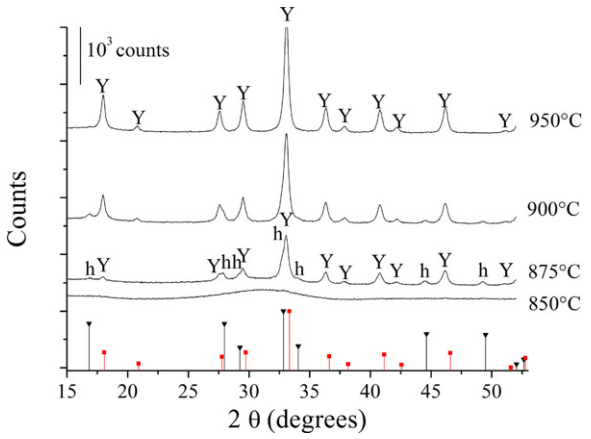

Fig. 1. HT-XRD showing the crystallisation behaviour between 850 °C and 950 °C. Y indicates the YAG phase (square markers), h the hexagonal transition phase $YAlO_3$ (triangular markers).

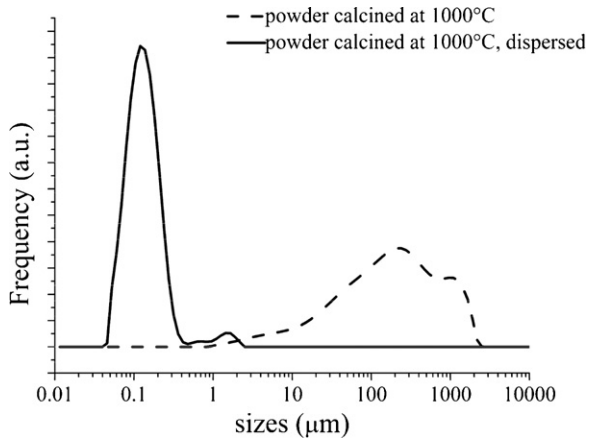

Fig. 3. Typical particle size distribution (by volume) before and after dispersion, regardless of the dispersion method.

The crystallite size, as calculated by Sherrer's method,[29] is about 30 nm for a calcination temperature of 1000 °C, while significantly increasing, to 65 nm size, at 1200 °C. The pre-treatment temperature of 1000 °C was thus selected for this study.

The calcined powder presented coarse agglomerates (insert in Fig. 4), with a mean size of about 100 μm, which were effectively reduced by both the dispersion routes tested, i.e. ball milling (BM) and ultrasonication (US). In fact, a sharp, monomodal particle distribution was achieved after dispersion, presenting a mean agglomerate size of about 120 nm (Fig. 3).

The dispersion process was considered completed when the 90% of the cumulative size distribution (by volume) was below 300 nm, a threshold reached after about 1 h and 6 h for US and BM, respectively. A transmission electron microscopy (TEM) image of the dispersed particles is presented in Fig. 4.

Sintering was carried out at different temperatures, following the cycle described above. Very different results were obtained for the BM and the US powder, with much higher transmittance values recorded for the US powder. The best sintering temperature for obtaining a high transmittance material was not the same for BM or US dispersed powder. Indeed, the best result, in terms of transmittance in both the infrared and visible range, was obtained, for BM powder, at a sintering temperature of 1225 °C, while a higher temperature (1325 °C) was best suitable for US dispersed powder (Table 2).

The transmittance for the infrared and the visible range as a function of the dispersion method is presented in Fig. 5.

SEM micrographs allow to appreciate the highly homogeneous and dense YAG microstructure. The material obtained from the BM powder presents a mean grain size of 360 ± 20 nm (Fig. 6). Elongated pores of 100–200 nm size are observed. In the insert of Fig. 6, a micrograph of the thermally etched sample (1175 °C, 1 h) is presented. Energy dispersive X-ray analysis (EDX) was performed on points A and B. Atomic % of the elements were calculated. Atomic % ratio Y:Al is 0.4 in point A and 0.58 in point B (close to the expected 0.6 value for YAG). Point A revealed therefore an Al-rich stoichiometry.

For the US powder sintered at 1325 °C, the grain size is 330 ± 50 nm (Fig. 7). In this case intragranular pores (white arrows) have been observed, as well as intergranular ones (black arrows). However, it should be pointed out that their size does not exceed 50 nm. In the insert of Fig. 7, the fracture surface is shown.

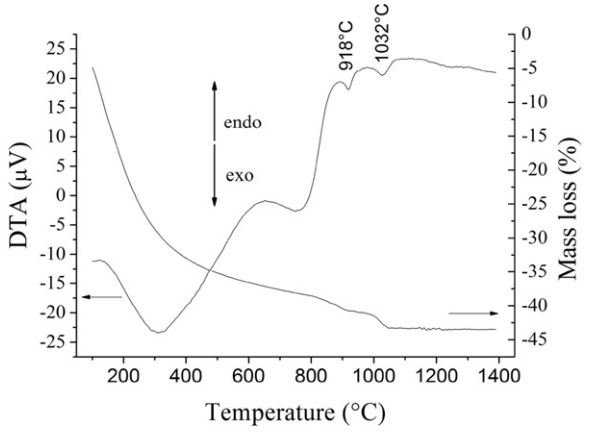

Fig. 2. DTA–TG curves of the as dried YAG precursor.

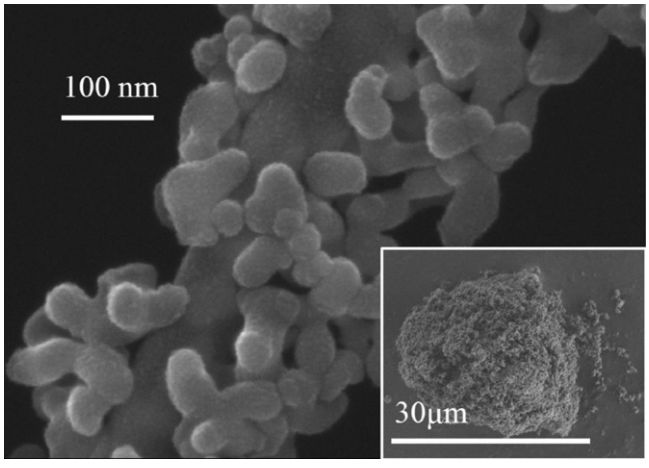

Fig. 4. TEM micrograph of YAG powder US dispersed. Agglomerated, as-calcined powder in the insert.

Table 2
Density, grain size and real in-line transmission (RIT), at 600 nm and 1064 nm, for transparent YAG.

Dispersion method	SPS sintering temp. (°C)	Density over the theoretical density [4.55 g/cm^3] (%, ±0.5)	Mean grain size (μm)	RIT at 600 nm for 1 mm thickness (%, ±0.5)	RIT at 1064 nm for 1 mm thickness (%, ±0.5)
US	1300	99.84	–	26.16	59.31
	1325	99.99	0.33 ± 0.05	66.29 (annealing 900 °C)	79.69 (annealing 950 °C)
	1350	99.99	1.99 ± 0.06	54.69 (annealing 800 °C)	77.00 (annealing 800 °C)
	1400	99.99	9.79 ± 1.89	23.34	73.04
BM	1200	99.78	–	2.48	27.95
	1225	99.33	0.360 ± 0.02	13.77	47.88
	1250	99.99	–	13.07	46.6
	1300	99.78	–	1.39	21.14

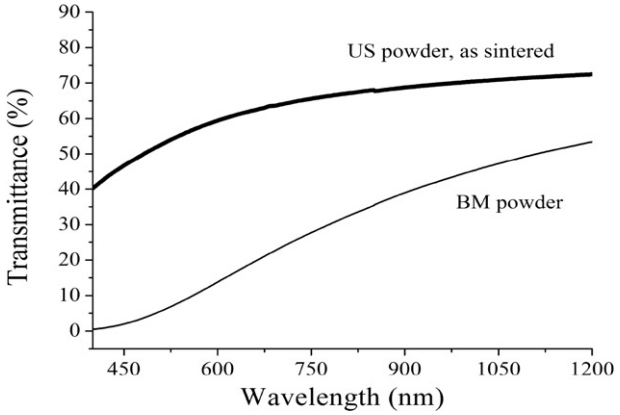

Fig. 5. Transmittance in the visible and infrared range as a function of the dispersion method (only the best results for each method are shown).

Samples from US powder sintered at higher temperatures have also been observed. As expected, the grain size increases. For a sintering temperature of 1350 °C the grain size is about 2 μm, with small pores of about 20 nm in size (Fig. 8, insert). At 1400 °C exaggerated grain growth occurs, accompanied by pore coarsening. Grains and intragranular pores as large as 15 and 1 μm, respectively, were observed.

Samples from US powders were submitted to air annealing. The results for US YAG 1 mm thick, sintered at 1325 °C, are presented in Fig. 9. The small leaps at 850 nm are due to the different detectors used inside the spectrophotometer, in the corresponding wavelength range. A PMT detector is used for the UV–VIS range, while a Peltier-cooled PbS detector is provided in the NIR region [Jasco specifications].

The annealing procedure led to a brighter colour of the samples subjected to thermal treatment (Fig. 10). The best transmittance in the wavelength range <600 nm was achieved after annealing at 900 °C, while higher temperatures were detrimental to transmittance at low wavelengths, as the sample turned opaque. Transmittance in the infrared range, on the opposite, was increased for all the annealing studied temperatures.

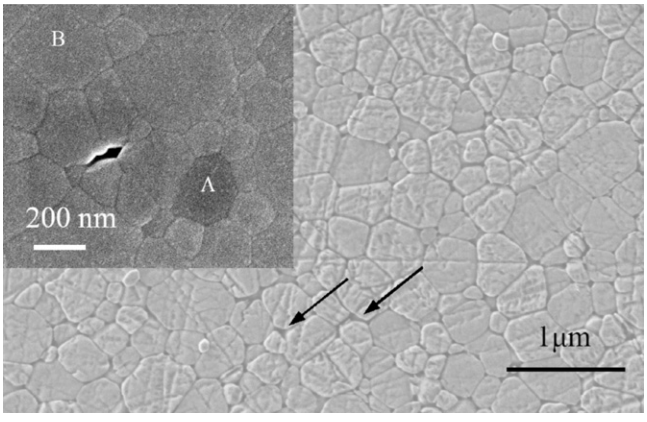

Fig. 6. Microstructure of YAG obtained from BM powder, sintered at 1225 °C, chemically and thermally (insert) etched.

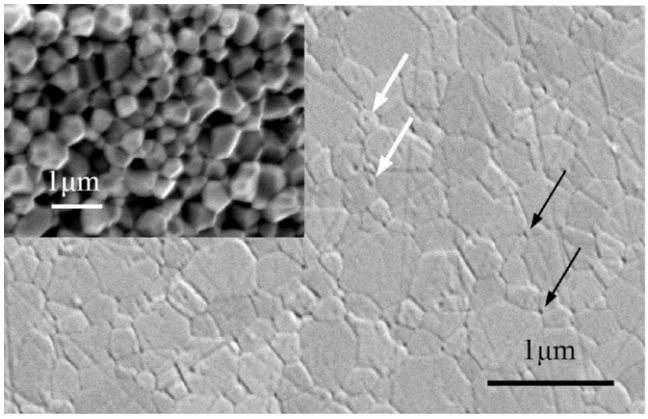

Fig. 7. Microstructure of YAG obtained from US powder, sintered at 1325 °C.

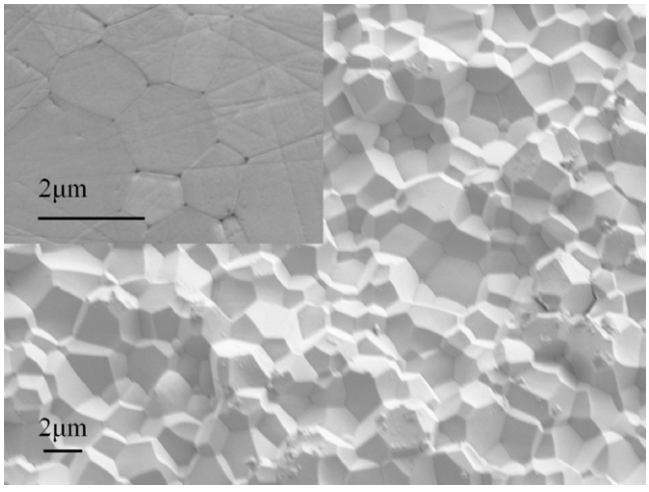

Fig. 8. Microstructure of YAG obtained from US powder, sintered at 1350°.

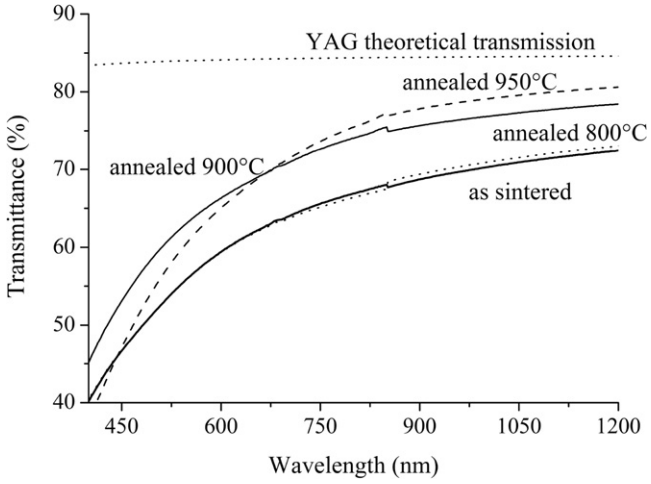

Fig. 9. transmittance of the sample sintered at 1325 °C (thick line), after annealing at 800 °C (dotted line, almost no change is detectable), at 900 °C (solid line, higher transmittance for wavelengths <700 nm) and after annealing at 950 °C (long dash line, higher transmittance for wavelengths >700 nm).

The results for density (Archimedes' method), mean grain size, transmittance in the visible and in the infrared range are summarized in Table 2 as a function of the sintering temperature and of the dispersion method. The US sample sintered at 1300 °C is inhomogeneous, being the centre much darker than the borders. The measurement was taken at the sample's centre.

4. Discussion

By observing results reported in Table 2, it is clear that samples from BM powder show lower transmittance and density than the ones from US powder. Part of this difference can be explained with the different sintering temperature applied for the two powders. However, even when the sintering temperature of BM powder was raised, no improvement in terms of density and transmittance was found. The larger size of the pores in the BM sample can explain the loss of transmittance, particularly in the visible range.

It has been shown that for dense metal oxides of the same porosity, an increasing pore diameter has a detrimental effect on

Fig. 10. Sample from US powder, sintered at 1350 °C, before (left) and after (right) annealing at 800 °C for 1 h in air. The two samples are 1.4 and 1.3 mm thick.

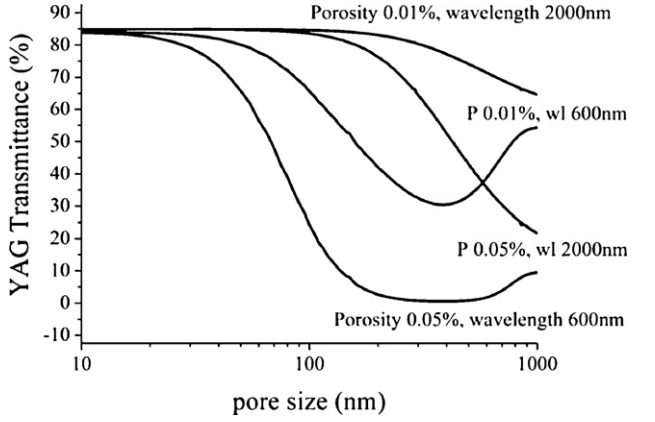

Fig. 11. YAG transmittance as a function of pore size, at wavelength 600 nm and 2000 nm, for porosity 0.01% and 0.05%.

their optical characteristics.[30,31] We calculated the effect of the pore size mean diameter on the in-line transmission, using the Beer–Lambert law:

$$T = T_{th}\ \exp(-\gamma t)$$

where *Tth* is the theoretical transmittance, γ is the extinction coefficient and t is the sample thickness.

The extinction coefficient γ is the sum of the contributions of the grain boundaries and of the pore scattering.[27] As YAG is a monorefrigent material, with a symmetric cubic cell,[32] no influence of the grain size on transparency is expected, and the grain boundary scattering can be neglected, leading to:

$$\gamma = \frac{3pC_{sca}}{4\pi r^3}$$

p is the porosity of the specimen, r is the mean radius of the pores, C_{sca} is the scattering cross section of one spherical pore and it can be calculated numerically using the Mie scattering theory.[33] The scattering cross section of pores C_{sca} has been determined for incident light of two wavelengths, 600 nm and 2000 nm, as a function of the mean pore size, by using the computer program given by Bernhard.[34] The scattering coefficient due to the pores can thus be determined. The in-line transmission is calculated as a function of the pore size, for the two wavelengths, for different amounts of porosity and for a sample thickness of 1.5 mm.

The results of the calculation are presented in Fig. 11. As expected, the in-line transmission depends not only on the porosity but is very sensitive to the pore diameter. When the pore size becomes of the same order of magnitude of the wavelength of the incident light, the transmission reaches a minimum. For a porosity of 0.01%, at the wavelength 600 nm, the transmission decreases significantly (RIT from 84% to 65%) if the pore size exceeds 100 nm, whereas at 2000 nm, the same decrease occurs for a pore size higher than about 1 μm.

The difficulty in eliminating pores in the BM YAG could be explained by the presence of pollution coming from the milling media. It can be supposed that alumina debris either hinder the densification, because of their non-spherical shape, or segregate as second phases, thus reducing transmittance because of their different refractive index. Partial evidence of

this hypothesis can be identified in the presence of grains with a Al-rich stoichiometry (insert of Fig. 6).

On the basis of the measured porosity and pore size of US YAG, a higher transmittance is expected. Carbon contamination and/or oxygen vacancies are the most probable factors causing transmittance loss for SPS-sintered samples.[35,36] Oxygen vacancies are formed in the reducing atmosphere of the SPS chamber during sintering, while carbon contamination arises out of diffusion from the graphite die. Annealing in air has an effect on both oxygen vacancies and carbon particles. Post-SPS annealing in various environments has been successfully tested for some oxide ceramics,[36,37] but to the best of our knowledge its effectiveness for SPS sintered YAG had not yet been tested.

The higher transmittance recorded after annealing in air can be due to oxygen vacancies removal, as suggested by Lee et al.[19] The lower transmittance in the range 300–600 nm, recorded after annealing at 950 °C, could be due to evaporation of carbon particles, leaving behind tiny pores in the bulk, or to microstructural changes during annealing, leading to new or larger defects.[38]

5. Conclusions

Co-precipitation of chlorides in ammonium bicarbonate led to a YAG precursor which was calcined and effectively dispersed by ultrasonication, resulting in a fine and well sinterable YAG powder.

Ultrasonic dispersion proved to be a suitable dispersion method for obtaining transparent samples, while only translucent samples were obtained from ball milled powder.

The appropriate handling of the powder led to a fine grained (330 nm), transparent (66% at 600 nm for 1 mm thickness) YAG ceramics. Spark plasma sintering has been applied, with a relatively short thermal cycle, followed by annealing in air, increasing the sample transmittance.

Our study demonstrates that, even if a coarse powder is obtained by oven drying, its size can be reduced by ultrasonic dispersion without significant drawbacks. Such a simple, low cost, method could be potentially extended to other materials, when sintering to transparency is required.

Acknowledgements

The authors wish to thank S. Cardinal, L. Lallemant and F. Mercier from INSA-Lyon and M. Raimondo from Politecnico di Torino for their part in the experimental work.

References

1. Nozawa H, Yanagitani T, Nishimura T, Tanaka H. Mechanical properties of fully dense yttrium aluminium garnet (YAG) ceramics. *J Ceram Soc Jpn* 2008;**116**:649–52.
2. Mezeix L, Green DJ. Comparison of the mechanical properties of single crystal and polycrystalline yttrium aluminum garnet. *Int J Appl Ceram Technol* 2006;**3**:166–76.
3. Ikesue A, Aung YL. Ceramic laser materials. *Nat Photonics* 2008;**2**:721–7.
4. Liu M, Lu Y, Xie ZB, Chow GM. Enhancing near-infrared solar cell response using upconverting transparent ceramics. *Sol Energy Mater Sol Cells* 2011;**95**:800–3.
5. Yagi H, Yanagitani T, Numazawa T, Ueda K. The physical properties of transparent $Y_3Al_5O_{12}$ elastic modulus at high temperature and thermal conductivity at low temperature. *Ceram Int* 2007;**33**:711–4.
6. Tong S, Lu T, Guo W. Synthesis of YAG powder by alcohol–water co-precipitation method. *Mater Lett* 2007;**61**:4287–9.
7. Rashmi Singh, Khardekar RK, Arun Kumar, Kohli DK. Preparation and characterization of nanocrystalline Nd-YAG powder. *Mater Lett* 2007;**61**:921–4.
8. Nien Y-T, Chen Y-L, Chen I-G, Hwang C-S, Su Y-K, Chang S-J, et al. Synthesis of nano-scaled yttrium aluminum garnet phosphor by co-precipitation method with HMDS treatment. *Mater Chem Phys* 2005;**93**: 79–83.
9. Deineka TG, Doroshenko AG, Mateychenko PV, Tolmachev AV, Vovk EA, Vovk OM, et al. Influence of sulfate ions on properties of co-precipitated $Y_3Al_5O_{12}$:Nd_{3+} nanopowders. *J Alloys Compd* 2010;**508**:200–5.
10. Xu G, Zhang X, He W, Liu H, Hong L, Boughton RI. Preparation of highly dispersed YAG nano-sized powder by co-precipitation method. *Mater Lett* 2006;**60**:962–5.
11. Gong H, Tang D-Y, Huang H, Ma J. Agglomeration control of Nd:YAG nanoparticles via freeze drying for transparent Nd:YAG ceramics. *J Am Ceram Soc* 2009;**92**:812–7.
12. Suarez M, Fernandez A, Menéndez JL, Torrecillas R. Transparent yttrium aluminium garnet obtained by spark plasma sintering of lyophilized gels. *J Nanomaterials* 2009 [article number 138490].
13. Esposito L, Piancastelli A, Costa AL, Serantoni M, Toci G, Vannini M. Experimental features affecting the transparency of YAG ceramics. *Opt Mater* 2011;**33**:713–21.
14. Gong H, Tang D, Huang H, Ma J. Fabrication of yttrium aluminum garnet transparent ceramics from yttria nanopowders synthesized by carbonate precipitation. *J Electroceram* 2009;**23**:89–93.
15. Lu J, Ueda K-i, Yagi H, Yanagitani T, Akiyama Y, Kaminskii AA. Neodymium doped yttrium aluminum garnet ($Y_3Al_5O_{12}$) nanocrystalline ceramics-a new generation of solid state laser and optical materials. *J Alloys Compd* 2002;**341**:220–5.
16. Liu W, Zhang W, Li J, Kou H, Zhang D, Pan Y. Synthesis of Nd:YAG powders leading to transparent ceramics: the effect of MgO dopant. *J Eur Ceram Soc* 2011;**31**:653–7.
17. Stevenson AJ, Li X, Martinez MA, Anderson JM, Suchy DL, Suchy DL, et al. Effect of SiO_2 on densification and microstructure development in Nd:YAG transparent ceramics. *J Am Ceram Soc* 2011;**94**:1380–7.
18. Khazanov EA. Thermally induced birefringence in Nd:YAG ceramics. *Opt Lett* 2002;**27**:716–8.
19. Lee S-H, Kupp ER, Stevenson AJ, Anderson JM, Messing GL, Li X, et al. Hot isostatic pressing of transparent Nd:YAG ceramics. *J Am Ceram Soc* 2009;**92**:1456–63.
20. Frage N, Kalabukhov S, Sverdlov N, Ezersky V, Dariel MP. Densification of transparent yttrium aluminum garnet (YAG) by SPS processing. *J Eur Ceram Soc* 2010;**30**:3331–7.
21. Anselmi-Tamburini U, Garay JE, Munir ZA. Fast low-temperature consolidation of bulk nanometric ceramic materials. *Scr Mater* 2006;**54**:823–8.
22. Orrù R, Licheri R, Locci AM, Cincotti A, Cao G. Consolidation/synthesis of materials by electric current activated/assisted sintering. *Mater Sci Eng Rep* 2009;**63**:127–287.
23. Chaim R, Levin M, Shlayer A, Estournes C. Sintering and densification of nanocrystalline ceramic oxide powders: a review. *Adv Appl Ceram* 2008;**107**:159–69.
24. Chaim R, Kalina M, Shen JZ. Transparent yttrium aluminum garnet (YAG) ceramics by spark plasma sintering. *J Eur Ceram Soc* 2007;**27**: 3331–7.
25. Suárez M, Fernández A, Menéndez JL, Nygren M, Torrecillas R, Zhao Z. Hot isostatic pressing of optically active Nd:YAG powders doped by a colloidal processing route. *J Eur Ceram Soc* 2010;**30**:1489–94.
26. Liu J, Yao W, Kear B, Mukherjee AK. Microstructure and IR transmittance of yttria–magnesia (50:50 vol%) nano-composites consolidated from agglomerated and ultrasonic horn treated nano-powders. *Mater Sci Eng B* 2010;**171**:149–54.
27. Apetz R, van Bruggen MPB. Transparent alumina: a light-scattering model. *J Am Ceram Soc* 2003;**86**:480–6.

28. Li JG, Ikegami T, Lee JH, Mori T, Yajima Y. Co-precipitation synthesis and sintering of yttrium aluminum garnet (YAG) powders: the effect of precipitant. *J Eur Ceram Soc* 2000;**20**:2395–405.
29. Zak AK, Majid WHA, Abrishami ME, Yousefi R. X-ray analysis of ZnO nanoparticles by Williamson-Hall and size-strain plot methods. *Solid State Sci* 2011;**13**:251–6.
30. Krell A, Klimke J, Hutzler T. Transparent compact ceramics: inherent physical issues. *Opt Mater* 2009;**31**:1144–50.
31. Bonnefont G, Fantozzi G, Trombert S, Bonneau L. Fine-grained transparent $MgAl_2O_4$ spinel obtained by spark plasma sintering of commercially available nanopowders. *Ceram Int* 2012;**38**:131–40.
32. Pawlak, et al. ESCA studies of yttrium aluminum garnet. *J Phys Chem B* 1999;**103**:1454–61.
33. van de Hulst HC. *Light scattering by small particles*. New York: Dover Publications; 1981.
34. Bernhard, M., http://www.lightscattering.de/MieCalc/index.html.
35. Bernard-Granger G, Benameur N, Guizard C, Nygren M. Influence of graphite contamination on the optical properties of transparent spinel obtained by spark plasma sintering. *Scr Mater* 2009;**60**:164–7.
36. Jiang DT, Hulbert DM, Anselmi-Tamburini U, Ng T, Land D, Mukherjee AK. Optically transparent polycrystalline Al_2O_3 produced by spark plasma sintering. *J Am Ceram Soc* 2008;**91**:151–4.
37. Anselmi-Tamburini U, Garay JE, Munir ZA, Tacca A, Maglia F, Chiodelli G, et al. Spark plasma sintering and characterization of bulk nanostructured fully stabilized zirconia: part II. Characterization studies. *J Mater Res* 2004;**19**:3263–9.
38. Zhang H, Kim BN, Morita K, Yoshida H, Lim J-H, Hiraga K. Optical properties and microstructure of nanocrystalline cubic zirconia prepared by high-pressure spark plasma sintering. *J Am Ceram Soc* 2011;**94**: 2981–6.